The spin structure of the nucleon

Eva-Maria Kabuss

Inst. für Kernphysik, Mainz University, D-55099 Mainz, Germany

An introduction to deep inelastic scattering experiments investigating the spin structure of the proton and the neutron is given. Discussed are measurements with longitudinally polarised targets to determine the spin structure function g_1 and sum rules and to do pQCD analyses with inclusive data, while a flavour separation and first extractions of the gluon polarisation are performed with semi-inclusive data.

PACS: 13.60.Hb, 13.88.+i
Key words: deep inelastic scattering, structure functions, gluon polarisation

1 Introduction

Experiments investigating the spin structure of the nucleon started in the seventies with deep inelastic scattering experiments off polarised protons at SLAC and later at CERN by the EMC. One of the exciting findings was that the contribution of the quarks to the nucleon spin is much smaller than anticipated before [1]. These results initiated a series of experiments at CERN, SLAC, DESY and later also at JLAB (see table 1) studying the spin structure of protons and neutrons in much more detail. All these experiments support the original finding that the contribution of the quarks to the nucleon spin is of the order of 25 %. Thus, other contributions are neccessary to solve the spin puzzle of the nucleon:

$$S_{\mathrm{p}} = \frac{1}{2} = \frac{1}{2}\Delta\Sigma + \Delta G + L_{\mathrm{q}} + L_{\mathrm{G}}\,.$$

Here, $\Delta\Sigma = \Delta u + \Delta d + \Delta s$ is the contribution of quarks, ΔG the contribution of gluons and $L_{\mathrm{q,G}}$ their orbital angular momenta.

In this lecture I will give an introduction to the experiments studying the quark and gluon polarisations and discuss the recent measurements of the spin structure function g_1, the separation of the different quark flavours and first measurements of ΔG. Measurements of the second spin structure function g_2 will not be covered (but see [2]).

To complete the picture of the nucleon, additional knowledge of the transverse quark distributions is required, which can be accessed in semi-inclusive measurements using transversely polarised targets. Measurements of the orbital angular momentum have not yet been done, but may be accessed by measuring generalised parton distributions in exclusive reactions like deeply virtual Compton scattering. These topics are discussed in the contribution by K. Rith [3].

2 Inclusive measurements

2.1 Cross sections and asymmetries

To investigate the spin structure of the nucleon polarised leptons are scattered off polarised nucleons. The kinematics of the corresponding one-photon exchange process are shown in Fig. 1.

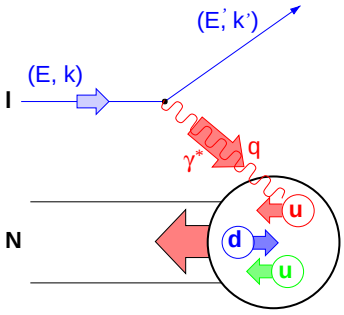

$$Q^2 = -(k-k')^2 =^{\text{lab}} 4EE' \sin^2\frac{\theta}{2}$$
$$\nu = \frac{P\cdot q}{2M} =^{\text{lab}} E - E'$$
$$x = \frac{Q^2}{2P\cdot q} =^{\text{lab}} \frac{Q^2}{2M\nu}$$
$$y = \frac{P\cdot q}{P\cdot k} =^{\text{lab}} \frac{\nu}{E}$$

Fig. 1. Deep inelastic lepton nucleon scattering in the quark parton modell

Here, Q^2 is the negative squared of the four-momentum transfer q by the virtual photon and ν the energy transfer in the laboratory system with $k = (E, \vec{k})$ and $k' = (E', \vec{k'})$ the four-momenta of the incoming and outgoing lepton. The two Lorentz invariant variables x and y range from 0 to 1. Here, y is the relative energy transfer, and x is interpreted as the momentum fraction carried by the struck quark in the quark parton modell [4]. M is the proton mass and θ the scattering angle in the laboratory system.

The cross section is given by the sum of the unpolarised cross section $\mathrm{d}\bar{\sigma}$ depending on the unpolarised structure functions $F_1(x,Q^2)$ and $F_2(x,Q^2)$ and the polarised contribution $\mathrm{d}\Delta\sigma$ depending on the spin structure functions $g_1(x,Q^2)$ and $g_2(x,Q^2)$. Measurements were done with longitudinally and transversly polarised targets yielding $\mathrm{d}\Delta\sigma_\parallel = \mathrm{d}\sigma^{\uparrow\downarrow} - \mathrm{d}\sigma^{\uparrow\uparrow}$ and $\mathrm{d}\Delta\sigma_\perp = \mathrm{d}\sigma^{\uparrow\rightarrow} - \mathrm{d}\sigma^{\uparrow\leftarrow}$. The first arrow depicts the lepton, the second one the target spin. In terms of structure functions the cross sections are given by

$$\frac{\mathrm{d}^3\bar{\sigma}}{\mathrm{d}x\mathrm{d}y\mathrm{d}\phi} = \frac{4\alpha^2}{Q^2}\left\{\frac{y}{2}F_1 + \frac{1}{2xy}\left(1-y-\frac{y^2\gamma^2}{4}\right)F_2\right\}$$
$$\frac{\mathrm{d}^3\Delta_\parallel\sigma}{\mathrm{d}x\mathrm{d}y\mathrm{d}\phi} = \frac{4\alpha^2}{Q^2}\left\{\left(1-y-\frac{y^2\gamma^2}{4}\right)g_1 - \frac{y}{2}\gamma^2 g_2\right\}$$
$$\frac{\mathrm{d}^3\Delta_\perp\sigma}{\mathrm{d}x\mathrm{d}y\mathrm{d}\phi} = \frac{4\alpha^2}{Q^2}\left\{\gamma\sqrt{1-y-\frac{y^2\gamma^2}{4}}\left(\frac{y}{2}g_1 + g_2\right)\right\}$$

with $\gamma = 2mx/Q^2$ and α the fine structure constant. The double spin asymmetries

$A = \Delta\sigma/2\bar{\sigma}$ are then given by

$$A_{\parallel}(x,Q^2) = \frac{d\sigma^{\uparrow\downarrow} - d\sigma^{\uparrow\uparrow}}{d\sigma^{\uparrow\downarrow} + d\sigma^{\uparrow\uparrow}} \quad \text{and} \quad A_{\perp}(x,Q^2) = \frac{d\sigma^{\uparrow\rightarrow} - d\sigma^{\uparrow\leftarrow}}{d\sigma^{\uparrow\rightarrow} + d\sigma^{\uparrow\leftarrow}}\,.$$

In this lecture, only measurements with longitudinally polarised targets are discussed. The corresponding longitudinal asymmetry $A_{\parallel}$ can be interpreted in terms of the absorption of transversely polarised photons with the spin parallel ($\sigma_{3/2}$) or antiparallel ($\sigma_{1/2}$) to the nucleon spin. Figure 2 shows a quark parton modell interpretation. Here, the photon nucleon asymmetry $A_1 = (\sigma_{1/2} - \sigma_{3/2})/(\sigma_{1/2} + \sigma_{3/2})$

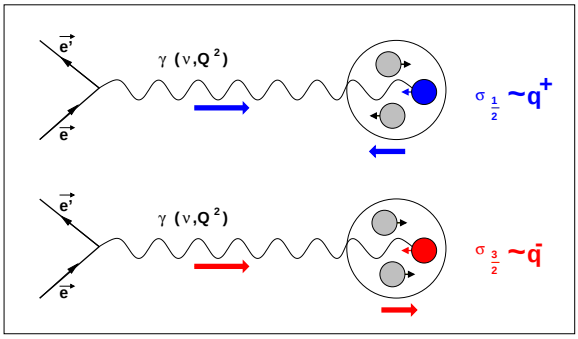

Fig. 2. Absorption of polarised photons on polarised nucleons in the quark parton modell.

is given in terms of the distribution of quarks with the spin parallel, $q^+(x)$, or antiparallel, $q^-(x)$, to the nucleon spin

$$A_1 \approx \frac{\Sigma_q\, e_q^2\, (q(x)^+ - q(x)^-)}{\Sigma_q\, e_q^2\, (q(x)^+ + q(x)^-)} = \frac{g_1(x)}{F_1(x)}.$$

Thus, A_1 measures the charge waited sum of the quark contributions to the nucleon spin, i.e. the spin structure function $g_1(x)$.

The exact relation between the lepton nucleon asymmetry, $A_{\parallel}$, and the photon nucleon asymmetry, A_1, is given by

$$A_{\parallel} = D(A_1 + \eta A_2) = \frac{1}{F_1}(g_1 - \gamma^2 g_2),$$

where the polarisation transfer, D, from the lepton to the nucleon

$$D = \frac{y(2-y)}{y^2 + 2(1+R)(1-y)}$$

increases with the relative energy transfer y. $\eta = 2(1-y)\sqrt{Q^2}/(y(2-y)E)$ and γ are kinematic factors and $R = \sigma_{\mathrm{L}}/\sigma_{\mathrm{T}}$ is the cross section ratio for the absorption of longitudinally to transversely polarised photons.

The photon nucleon asymmetry $A_2(x, Q^2) = 2\,\sigma_{\mathrm{LT}}/(\sigma_{1/2} + \sigma_{3/2})$ is given by the interference between longitudinal and transverse contributions and has no simple parton modell interpretation. But measurements have shown that the second structure function g_2 is small [5]. Together with the fact that the kinematic factor in front is also small for most of the experiments, the second term for $A_\parallel$ can often be neglected so that

$$A_1 \approx \frac{g_1}{F_1} \approx \frac{A_\parallel}{D}.$$

The experimental asymmetry $A^{\mathrm{exp}} = p_{\mathrm{B}}\; p_{\mathrm{T}}\; f\; D\; A_1$ includes the target polarisation p_{T}, the beam polarisation p_{T}, the dilution factor f which gives the fraction of polarisable nucleons in the target material and is typically of the order of 10^{-2}.

2.2 Experiments

Up to know all inclusive spin structure measurements were performed at fixed target experiments ranging from 6 GeV electron beams at JLAB to the 200 GeV muon beam at CERN. Table 1 gives an overview about the experiments.

Table 1. List of polarised DIS experiments

SLAC	**E80, E130**	$\vec{\mathrm{e}}\,\vec{\mathrm{p}}$	≤ 20 GeV
CERN	**EMC**	$\vec{\mu}\,\vec{\mathrm{p}}$	100–200 GeV
SLAC	**E142, 143**	$\vec{\mathrm{e}}\,\vec{\mathrm{p}}, \vec{\mathrm{n}}, \vec{\mathrm{d}}$	≤ 28 GeV
CERN	**SMC**	$\vec{\mu}\,\vec{\mathrm{p}}, \vec{\mathrm{d}}$	100, 190 GeV
SLAC	**E154, 155**	$\vec{\mathrm{e}}\,\vec{\mathrm{p}}, \vec{\mathrm{n}}, \vec{\mathrm{d}}$	≤ 50 GeV
DESY	**HERMES**	$\vec{\mathrm{e}}\,\vec{\mathrm{p}}, \vec{\mathrm{n}}, \vec{\mathrm{d}}$	27.5 GeV
CERN	**COMPASS**	$\vec{\mu}\,\vec{\mathrm{d}}$	160 GeV
JLAB	**HALL A**	$\vec{\mathrm{e}}\,\vec{\mathrm{n}}$	6 GeV
JLAB	**CLAS**	$\vec{\mathrm{e}}\,\vec{\mathrm{p}}, \vec{\mathrm{d}}$	6 GeV
JLAB	**RSS**	$\vec{\mathrm{e}}\,\vec{\mathrm{p}}, \vec{\mathrm{d}}$	6 GeV

Most experiments use solid state targets polarised by dynamic nuclear polarisation at very low temperatures. The target materials were butanol, deuterated butanol, ammonia and ^{6}LiD yielding dilution factors between 0.1 and 0.4. In addition, ^{3}He is used as neutron target. Using a storage cell target with atomic hydrogen and deuterium, dilution factors of about 1 are reached by HERMES [6].

The experiments cover a kinematic range in Q^2 between 1 and 100 GeV^2 at high x, between 0.1 and 1 GeV^2 at x around 0.05 and only a very narrow range in Q^2 for the lowest x down to 10^{-4}.

2.3 Results for A_1 and g_1

The asymmetry A_1 was measured over the full kinematic range for the proton and the deuteron, while the ^{3}He measurements cover the smaller kinematic region accessible at SLAC and HERMES. Most experiments studied the x and Q^2 dependence of A_1. Up to now no Q^2 dependence of A_1 was observed [7, 8, 9], thus the data are usually averaged over Q^2 and their x dependence is studied.

Recently, a very precise measurement of $A_1^{\mathrm{d}}(x)$ was obtained by the HERMES collaboration [10]. The results are shown in Fig. 3 in comparison with previous measurements from SMC, E143 and E155. The high quality of this new data is clearly visible. On the bottom the average Q^2 for each of the data points is shown. The SLAC and HERMES data cover very similar Q^2 ranges with the HERMES data extending the x range by nearly a decade. The average Q^2 of the CERN muon experiments is generally higher by a factor of the order of 10. Their data also extend to much lower $x \approx 10^{-4}$. Meanwhile much improved data at low x were obtained by the COMPASS collaboration [9].

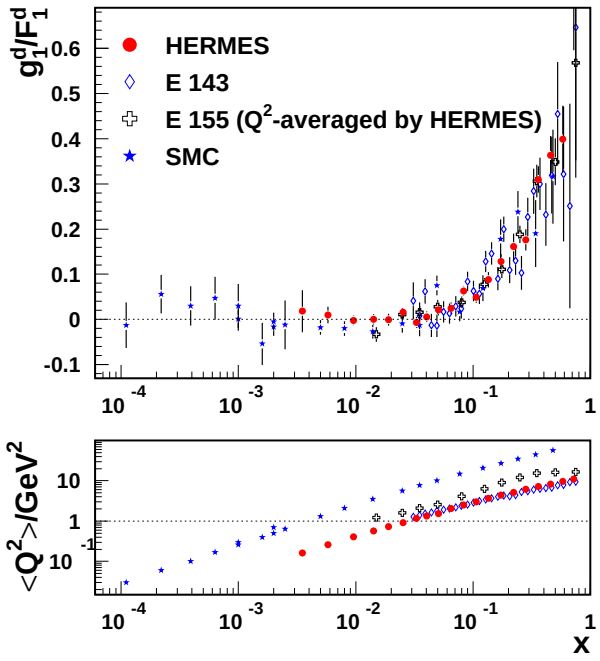

Fig. 3. Preliminary results for $g_1^{\mathrm{d}}/F_1^{\mathrm{d}}$ from HERMES compared to previous results from SLAC and SMC, the average Q^2 of the data points is given below.

From the measured asymmetries the spin structure function g_1 is extracted

$$g_1 = A_1 \cdot \frac{F_2}{2x(1+R)}$$

using parametrisations of the unpolarised structure functions, F_2 and R. Figure 4 left shows a compilation of the world data on g_1^{p}, g_1^{d} and g_1^{n} in the DIS region. Here, also three very accurate g_1^{n} points from JLAB E99-117 are included [11]. For the first time, these data show clearly the rise to positive values at high x.

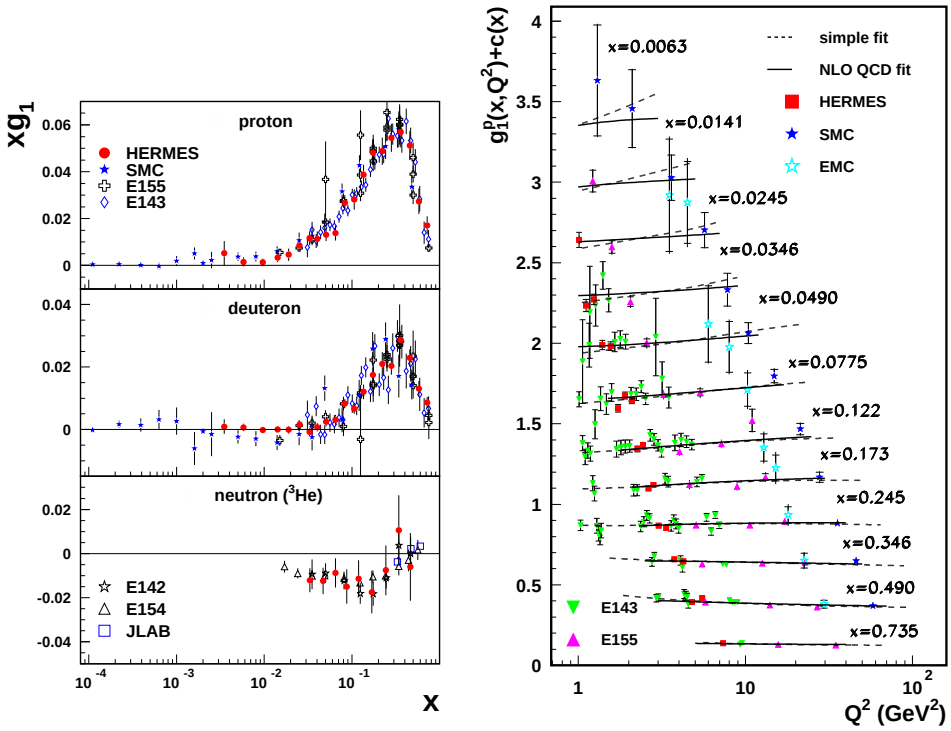

Fig. 4. Left: Compilation of results for xg_1 versus x for protons, deuterons and neutrons, Right: Q^2 dependence of g_1^p at fixed x.

2.4 QCD analysis

The interpretation of the results for g_1 in the DIS region is usually done in terms of a next-to-leading-order (NLO) perturbative QCD analysis. The DGLAP evolution equations [12] for the polarised parton densities are used to describe the Q^2 dependence of g_1 in terms of polarised singlett, $\Delta\Sigma = \sum_{i=1}^{n_f} \Delta q_i$, non-singlett, $\Delta q_{NS} = \sum_{i=1}^{n_f} \left(e_i^2/\langle e^2\rangle - 1\right) \Delta q_i$, and gluon distributions, Δg [13]:

$$\frac{\mathrm{d}}{\mathrm{d}\ln Q^2}\Delta q_{NS} = \frac{\alpha_s(Q^2)}{2\pi} \Delta P_{qq}^{NS} \otimes \Delta q_{NS}$$

$$\frac{\mathrm{d}}{\mathrm{d}\ln Q^2}\begin{pmatrix}\Delta\Sigma\\ \Delta g\end{pmatrix} = \frac{\alpha_s(Q^2)}{2\pi}\begin{pmatrix}\Delta P_{qq}^S & 2n_f\Delta P_{qg}\\ \Delta P_{gq} & \Delta P_{gg}\end{pmatrix}\otimes\begin{pmatrix}\Delta\Sigma\\ \Delta g\end{pmatrix}.$$

Alternatively valence quark, sea quark and gluon distribution can be used [14, 8]. The polarised splitting function, ΔP_{qq}, is equal to the unpolarised one, P_{qq}, leading to a very similar Q^2 dependence of g_1 and F_1 at high x, whereas $\Delta P_{qg} \neq P_{qg}$. Thus the Q^2 dependence of g_1 and F_1 may differ in the low x region.

The spin structure function g_1 is then calculated from the parton distributions with help of the coefficient functions C_{NS}, C_{S} and C_{g}

$$g_1(x,Q^2) = \frac{1}{2}\langle e^2\rangle \left[C_{NS} \otimes \Delta q_{NS} + C_S \otimes \Delta\Sigma + 2n_f C_g \Delta g\right]$$

where $\otimes$ denotes the convolution of the functions.

Clearly the parton distributions depend on the chosen renormalisation scheme. In most analysis the $\overline{\mathrm{MS}}$ scheme is used. In addition, the initial parametrisations for the parton distributions have to be chosen. For example

$$\Delta f_i(x,Q^2) = A_i\, x^{\alpha_i}\, (1+\gamma_i x^{\lambda_i})\, f_i(x,Q_0^2)$$

was used for the valence, sea and gluon distribtions in the recent AAC03 analysis [14] at the starting scale of $Q_0^2 = 1\,\mathrm{GeV}^2$. Here, $f_i(x,Q_0^2)$ denote the unpolarised distributions and A_i, α_i, γ_i and λ_i are fit parameters.

In Fig. 5 several recent analyses [15] are compared with the experimental results for g_1^{p}, g_1^{d} and g_1^{n}. The data are quite well described by all the analyses. The corresponding parton distributions are quite similar, too, especially for the valence quarks as shown in Fig. 6. Larger differences are observed for the sea quarks as they are much more correlated with the gluon distribution where the functional form is not constrained much by the data. This is due to the limited lever arm in Q^2 of the polarised data compared to the unpolarised ones especially in the low x range which is most sensitive to the gluon distribution (see also Fig. 4). From the analyses also the first moment of the singlett contribution can be estimated, e.g. a value of $\Delta\Sigma = 0.213 \pm 0.138$ at $Q^2 = 1\,\mathrm{GeV}^2$ is obtained in [14].

2.5 Sum rules

Much discussed results in polarised DIS are sum rules for structure functions. Using the first moments $a_q = \int_0^1 \Delta q(x)\mathrm{d}x$ of the polarised quark distributions, i.e. the contribution of quarks q to the nucleon spin, the first moment of g_1^{p} and g_1^{n} can be written as

$$\Gamma_1^{\mathrm{p,n}} = \int_0^1 g_1^{\mathrm{p,n}}(x)\mathrm{d}x = \pm\frac{1}{12}a_3 + \frac{1}{36}a_8 + \frac{1}{9}a_0\,.$$

The axial charges are related to the quark contributions by

$$\begin{aligned} a_3 &= a_{\mathrm{u}} - a_{\mathrm{d}} \\ a_8 &= a_{\mathrm{u}} + a_{\mathrm{d}} - 2a_{\mathrm{s}} \\ a_0 &= a_{\mathrm{u}} + a_{\mathrm{d}} + a_{\mathrm{s}}\ . \end{aligned}$$

Assuming isospin symmetry the Bjorken sum rule [16] is obtained for the difference of the proton and the neutron

$$\Gamma_1^{\mathrm{p}} - \Gamma_1^{\mathrm{n}} = \frac{1}{6}a_3 = \frac{1}{6}\left|g_{\mathrm{A}}/g_{\mathrm{V}}\right|^{\mathrm{n}\to\mathrm{p}}\ .$$

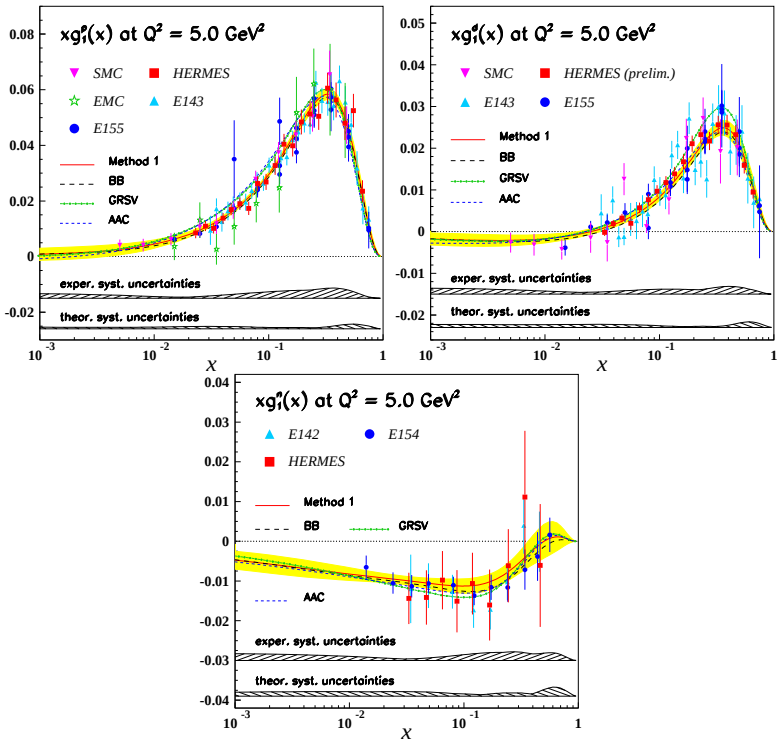

Fig. 5. Comparison of xg_1^{p}, xg_1^{d} and xg_1^{n} to recent QCD analyses [15].

Here, $a_3 = |g_{\mathrm{A}}/g_{\mathrm{V}}| = 1.267 \pm 0.0035$ [17] is measured in the neutron decay. Using in addition the $\mathrm{SU}(3)_{\mathrm{flavour}}$-symmetry in the baryon octett, a_8 can be determined from hyperon decays $a_8 = 3F - D = 0.585 \pm 0.023$. Neglecting a possible contribution from the strange quark sea, the Ellis-Jaffe sum rule [18] $a_0 = a_8 \approx 0.6$ is obtained for the contribution of the quarks to the nucleon spin.

Before comparing these predictions to experimental results, QCD corrections must be applied leading to:

$$a_0(Q^2)C_1^{\mathrm{S}}(Q^2) = \Delta\Sigma(Q^2)C_1^{\mathrm{S}}(Q^2) + \Delta G(Q^2)2n_{\mathrm{f}}C_1^{\mathrm{G}}(Q^2)\,,$$

$$\Gamma_1^{\mathrm{p,n}}(Q^2) = \frac{1}{12}\left(\frac{a_8}{3} \pm a_3\right)\, C_1^{\mathrm{NS}}(Q^2) + \frac{1}{9}\, a_0(Q^2)\, C_1^{\mathrm{S}}(Q^2)\,,$$

$$\Gamma_1^{\mathrm{p}} - \Gamma_1^{\mathrm{n}} = \frac{1}{6}\,|g_{\mathrm{A}}/g_{\mathrm{V}}| \cdot C_1^{\mathrm{NS}}(Q^2) = \frac{1}{6}a_3 \cdot C_1^{\mathrm{NS}}(Q^2)\,.$$

The recent E155 NLO QCD analysis [8] confirmed the validity of the Bjorken sum rule

$$\Gamma_1^{\mathrm{p}} - \Gamma_1^{\mathrm{n}} \;=\; 0.176 \pm 0.003 \pm 0.007$$

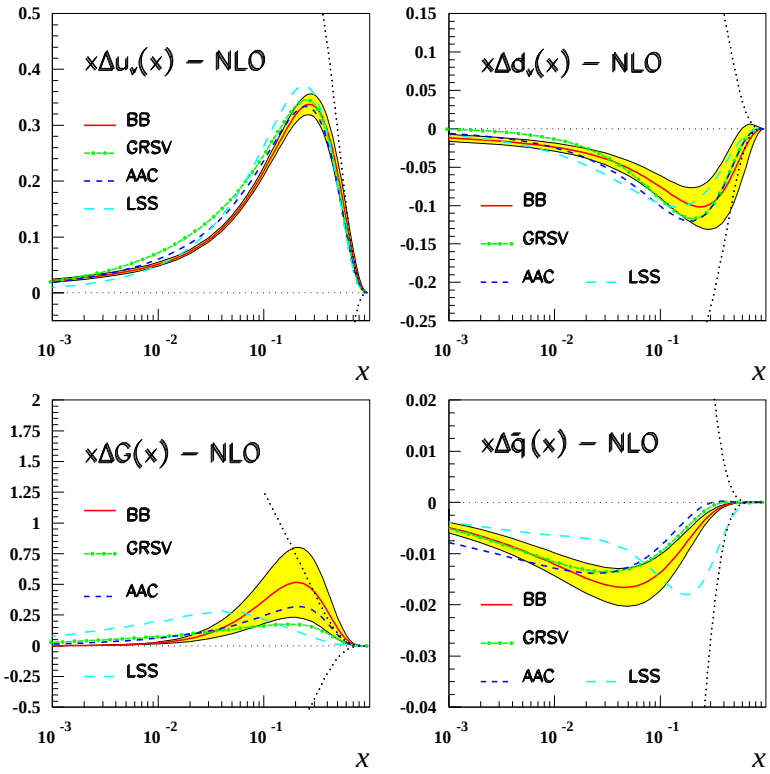

Fig. 6. Results for the polarised valence, gluon and sea distributions at $Q^2 = 4\,\mathrm{GeV}^2$ [15].

compared to the predicted value of $\Gamma_1^p - \Gamma_1^n = 0.181 \pm 0.005$ at $Q_0^2 = 5\,\mathrm{GeV}^2$. The first moments $a_g = 1.6 \pm 0.8$ (sta) ± 1.1 (sys) and $a_0 = 0.23 \pm 0.04$ (sta) $\pm$ 0.6 (sys) confirm the violation of the Ellis-Jaffe sum rule found in previous analyses.

2.6 Measurements in the resonance region

A new topic can be attacked if not only measurements in the DIS region are available but also in the resonance region. This is illustrated in Fig. 7 upper [19] where recent HERMES data on $A_1(x)$ in the resonance region are compared to data from the DIS region. The asymmetries show in general good agreement supporting the idea of quark-hadron-duality [20]. This duality is investigated further in much more detail in recent measurements by E01-006 (RSS) and CLAS EG1 at JLAB [21]. As an example Fig. 7 lower shows the CLAS results for g_1^p in the resonance region covering a large range in Q^2 from 0.26 to 3.8 GeV^2 from the elastic peak to $W \approx 2\,\mathrm{GeV}$ due to their large acceptance detector. Clear resonance structures are visible especially in the Δ-region indicated with triangles. The data are compared to a recent QCD fit to g_1 in the DIS region. The fit gives on average a good description of the resonance

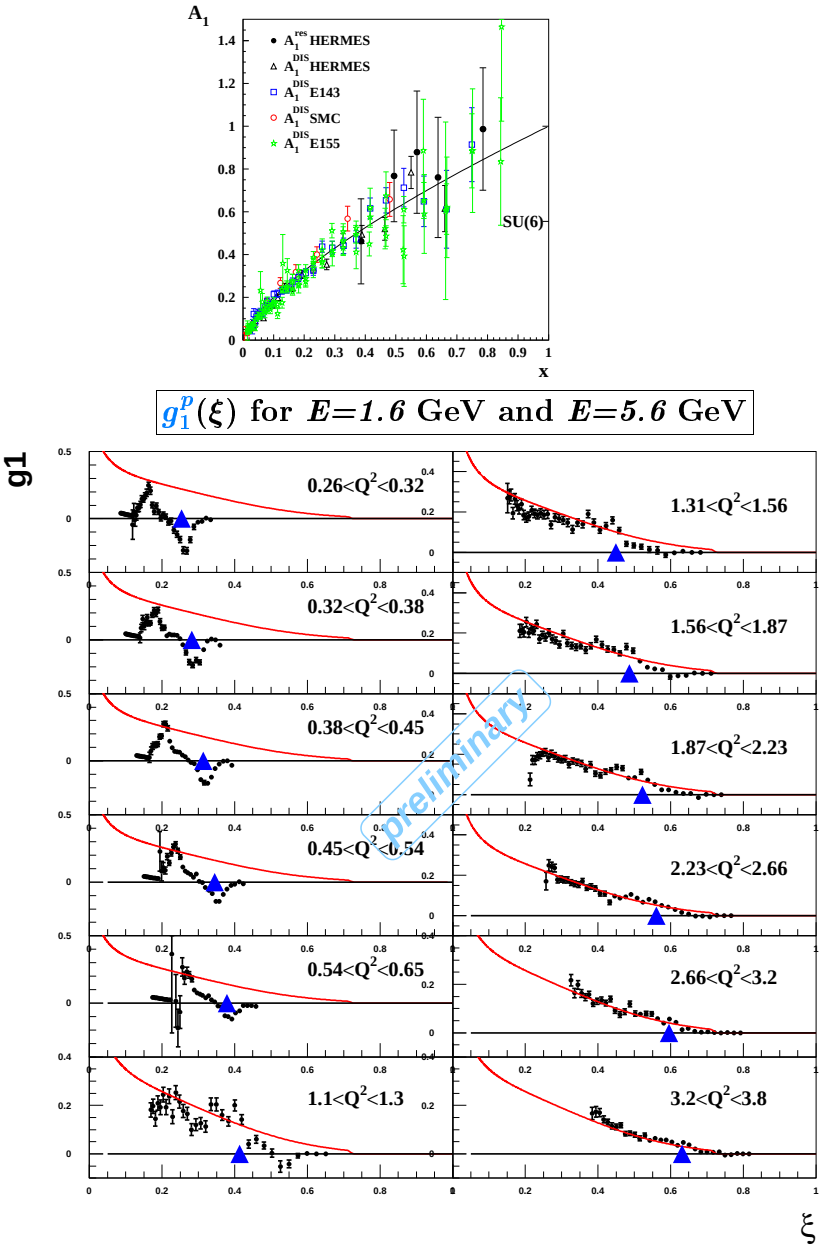

Fig. 7. Upper: Spin asymmetry A_1 as a function of x measured in the resonance region (full circles). The open symbols are results obtained in the DIS region. The curve represents a power law fit to the DIS data. Lower: $g_1^p(\xi)$ versus ξ with the Nachtmann variable $\xi = 2x(1+\sqrt{1+4M^2x^2/Q^2})^{-1}$ compared to a parametrisation of the DIS world data at $Q^2 = 10\,\mathrm{GeV}^2$. The $\Delta(1232)$ is indicated by the triangles.

data down to $Q^2 \approx 1\,\mathrm{GeV}^2$ except for the Δ-region where a clear violation of duality is observed.

3 Semi-inclusive measurements

3.1 Flavour decomposition

In inclusive measurements only the sum of all quark flavours is studied. For a flavour separation of the polarised quark distributions additional input data are needed. They can be obtained from semi-inclusive measurements as illustrated in Fig. 8 left. The leading hadron contains with a large probability the struck quark and thus

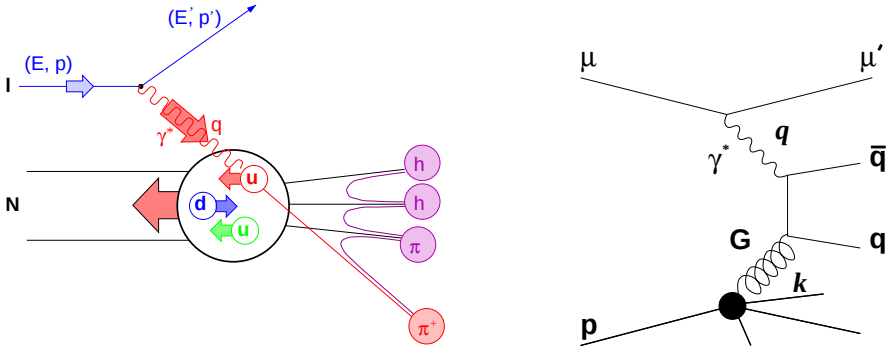

Fig. 8. Left: Semi-inclusive deep inelastic scattering, Right: photon gluon fusion.

carries information on the quark polarisation. The leading hadron is usually selected as the hadron with the largest z, where $z = E_\mathrm{h}/\nu$ is the fraction of the virtual photon energy carried by the hadron. In addition to this longitudinal variable, the hadron is also characterised by the transverse momentum, p_T, relative to the virtual photon direction arising from the intrinsic motion of the quarks in the nucleon and the fragmentation process from quarks to the final hadrons which is described by the fragmentation function, $D_\mathrm{q}^\mathrm{h}(z, Q^2)$. Measuring a hadron in addition to the scattered lepton, the semi-inclusive asymmetries

$$A_1^\mathrm{h} = \frac{\int \mathrm{d}z \sum_\mathrm{f} e_\mathrm{f}^2 \Delta q_\mathrm{f}(x, Q^2) \cdot D_\mathrm{f}^\mathrm{h}(z, Q^2)}{\int \mathrm{d}z \sum_\mathrm{f} e_\mathrm{f}^2 \; q_\mathrm{f}(x, Q^2) \cdot D_\mathrm{f}^\mathrm{h}(z, Q^2)}$$

are obtained, where z is chosen in the fragmentation region between 0.2 or 0.3 to 1. The fragmentation functions are used as weights to disentangle the different quark and antiquark flavours using the fact that the so called favoured fragmentation functions, e.g. $D_\mathrm{u}^{\pi^+}$, are larger the nonfavoured ones, e.g. $D_\mathrm{u}^{\pi^-}$. First measurements

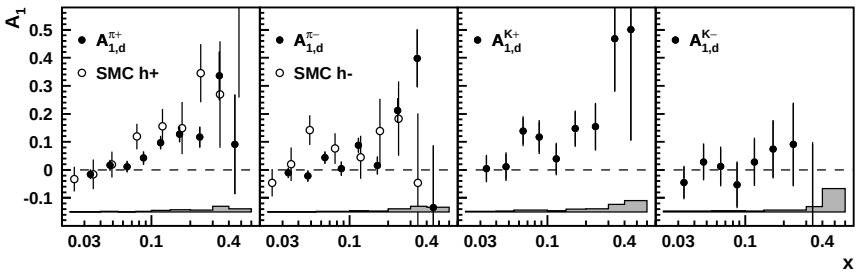

Fig. 9. The HERMES result for the semi-inclusive asymmetries $A_1^h(x)$ for π^+, π^-, K^+ and K^- obtained with a deuteron target compared to the previous SMC results for positive and negative hadrons.

were done by SMC for positive and negative hadrons from protons and deuterons [22]. More recent results were obtained by HERMES for positive and negative hadrons from protons and neutrons and identified pions and kaons from deuterons (see Fig. 9) [23]. The quark polarisations are then determined solving the system of linear equations using measured fragmentation functions (SMC) or fragmentation functions from Monte Carlo simulations (HERMES). In such a way the five quark distributions shown in Fig. 10 left were extracted. They are compared to recent parton parametrisations obtained from the pQCD analyses discussed above. The polarised u- and d-quark distributions are well determined and are positive resp. negative, while the three sea quark distributions are small and compatible with zero, with a slight tendency for a positive $\Delta s/s$. Also, a first attempt was made to study the flavour asymmetry in the light quark sea (see Fig. 9 right).

3.2 Gluon polarisation

In inclusive measurements the gluon polarisation can only be determined via scaling violations in the Q^2 dependence of g_1. Due to the limited precision and kinematical range of the existing data all these analyses result in rather large uncertainties for the gluon polarisation (see section 2.4), thus direct measurements are urgently needed.

In DIS the gluon distribution is accessible via the photon gluon fusion process (PGF) (see Fig. 8 right). Therefore, few years ago several activities were started to determine ΔG either from open charm production or from high p_T hadron pairs by SMC, HERMES and COMPASS. Alternatively the gluon polarisation can also be measured in collider experiments using polarised protons.

The measurement of $\Delta G/G$ via high p_T hadron pairs makes use of all PGF events $\gamma g \to q\bar{q}$ with all quark flavours q. To ensure a perturbative interpretation a hard scale is set by the requirement of a high transverse momentum p_T for the produced hadrons. To enhance PGF events the hadrons should have opposite charge and azimuth. Results for high p_T asymmetries were obtained by EMC [25], HER-

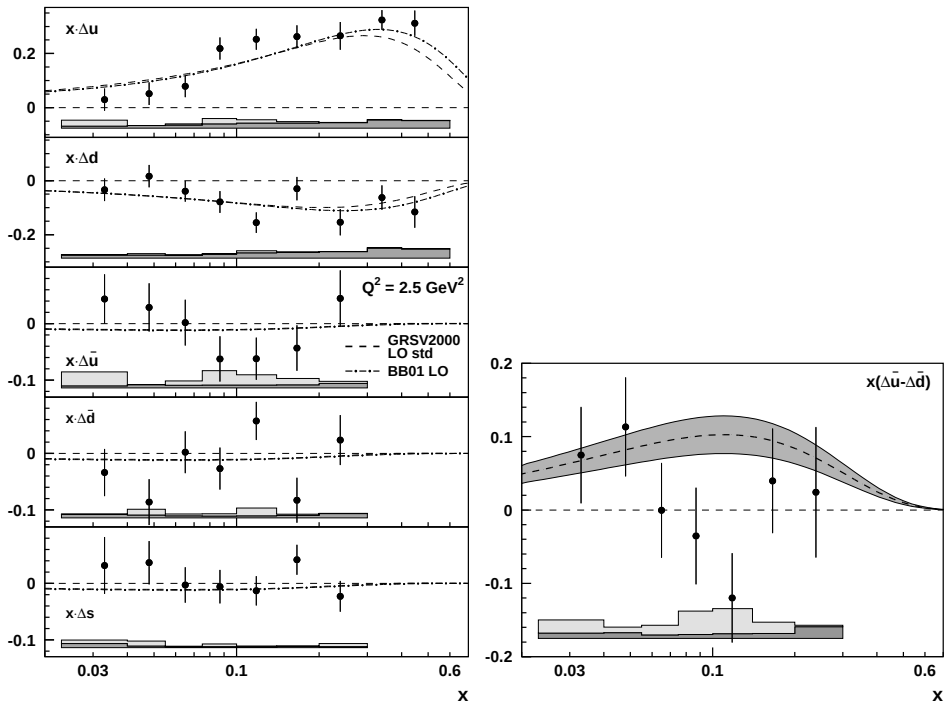

Fig. 10. Left: The quark helicity distributions $x\Delta q(x)$ at $Q^2 = 2.5\,\mathrm{GeV}^2$, Right: the flavour asymmetry in the helicity densities of the light sea.

MES [26] and COMPASS [27]. To extract $\Delta G/G$ from the measured asymmtries several background processes have to be accounted for (see Fig. 11) like the leading process (a), QCD Compton events (b), resolved photon processes and vector meson production. Thus, the measured asymmetry is

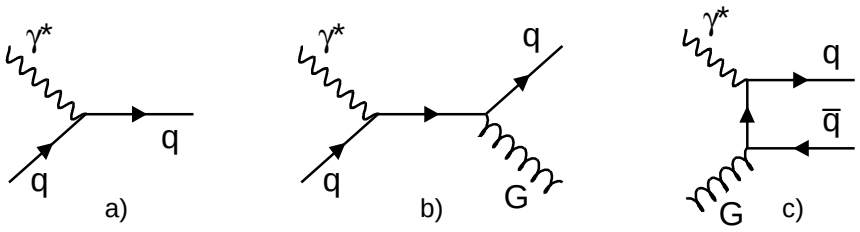

Fig. 11. Lowest order diagrams for γ^* absorption: a) leading process, b) QCD Compton and c) photon gluon fusion.

$$A_{\mathrm{LL}} \approx \langle a_{\mathrm{LL}}^{\gamma \mathrm{g} \longrightarrow \mathrm{qg}} \rangle \frac{\Delta q}{q} + \langle a_{\mathrm{LL}}^{\gamma \mathrm{g} \longrightarrow \mathrm{q\bar{q}}} \rangle \frac{\Delta G}{G} + \ldots\ldots$$

The relative contributions have to be determined by Monte Carlo simulations leading to an additional contribution to the systematic error. After all cuts the amount of PFG events is of the order of 25–30 % for all experiments. The results for $\Delta G/G$ are summarized in Fig. 12 left indicating that $\Delta G/G$ is probably not too large.

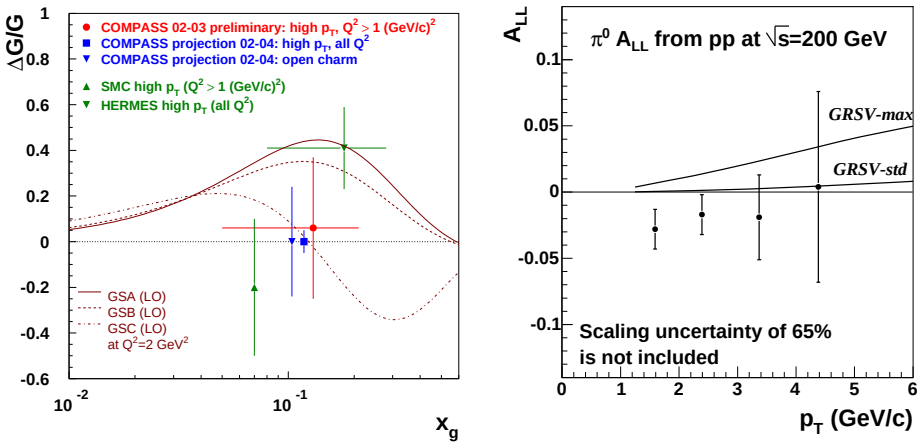

Fig. 12. Left: Results for $\Delta G/G$ from high p_{T} hadron pairs. In addition, the projection for the statistical accuracy for COMPASS from open charm production is shown. The curves show the parametrisations from [28]. Right: PHENIX A_{LL} data points versus p_{T} compared to theory calculations [36].

The alternative approach using open charm production followed by COMPASS uses a much cleaner signal. Here, only the processes $\gamma \mathrm{g} \rightarrow \mathrm{c\bar{c}}$ are selected by requiring charmed mesons (D^0, D^*) in the final state. The mass of the charm quark serves as hard scale, thus no p_{T} cut is neccessary. The mesons are reconstructed by their subsequent decays, e.g. $\mathrm{D}^0 \rightarrow \pi K$ (BR: 4 %). Unfortunately the branching ratios of the best channels are low. Also, due to the long solid state polarised target the reconstruction of the D meson decay vertex is not possible. They are reconstructed from the invariant mass distribution only. This method is hampered by a huge combinatorial background below the D^0 peak. Selecting D^* first by adding a slow π suppresses much of the background. An error of 0.24 for the gluon polarisation is expected for the COMPASS data from 2002 to 2004.

PHENIX [31] and STAR [29] at RHIC took data with longitudinally polarised protons in 2003 using 200 GeV protons with a polarisation of about 26 %. The integrated luminosity was about $0.2\,\mathrm{pb}^{-1}$. The final goal is the extraction of $\Delta G/G$ from prompt photon production $\mathrm{gq} \rightarrow \gamma \mathrm{q}$. Due to the limited statistics of this first longitudinal run the analysis started with other channels. STAR studied $\mathrm{gq} \rightarrow$

gq $\rightarrow$ 2 jets [30] and PHENIX gq $\rightarrow$ gq $\rightarrow \pi^0 X$ [33]. While the STAR analysis is still ongoing, results were obtained for π^0 asymmetries from PHENIX. The π^0 reconstruction makes use of the electromagnetic calorimeter which allows to access the central rapidity region. The unpolarised π^0 production cross section was determined and shows good agreement with NLO pQCD calculations for the whole range of transverse momenta [32]. The observed asymmetries, A_{LL}, are small and slightly negative, but still compatible with zero [33]. Several hard subprocesses like gg $\rightarrow$ gg and gq $\rightarrow$ gq contribute to π^0 production. The processes most important at central rapidities have a positive partonic asymmetry. Therefore is seems difficult to reconcile the data with any predictions [34, 35] if they are taken at their face values. This illustrates the potential of the π^0 measurements to constrain ΔG, when the data are improved with further measurements.

4 Summary

Spin physics is a very active field as well as in fixed target DIS experiments as in pp-collider experiments. Until now mainly inclusive DIS measurements were done yielding results for spin structure functions. High precision data are available allowing detailed NLO pQCD analyses and the determination of sum rules. At present, most emphasis lies on semi-inclusive DIS measurements. Data with longitudinally polarised targets are used to perform a separation of quark flavours and a determination of the gluon polarisation. Semi-inclusive measurements with transversely polarised targets have been started to extract the transverse quark distributions. Transversity and the gluon polarisation are also investigated in polarised pp-collider experiments at RHIC.

This work was supported by the Bundesministerium für Bildung und Forschung.

References

[1] EMC, J. Ashman et al.: Phys. Lett. B**206** (1988) 364.

[2] K. Kramer: *Proceedings of the 12th International workshop on Deep Inelastic Scattering and QCD (DIS04)*, Strbske Pleso (2004).

[3] K. Rith: these proceedings.

[4] see e.g. F. Halzen and A. D. Martin: *Quarks & Leptons*, Wiley & Sons, New York (1984).

[5] E155, P. L. Anthony et al.: Phys. Lett. B**553** (2003) 18.

[6] HERMES, K. Ackerstaff et al.: Nucl. Instr. Meth. A**417** (1998) 230.

[7] SMC, B. Adeva et al.: Rev. D**58** (1998) 112001.

[8] E155, P. L. Anthony et al.: Phys. Lett. B**493** (2000) 19.

[9] COMPASS, E. Ageev et al.: Phys. Lett. B**612** (2005)154.

[10] HERMES, C. Riedl: *Proc. of the 16th International Spin Symposium (SPIN04)*, Trieste (2004).

[11] E99-117, X. Zheng et al.: Phys. Rev. Lett. **92** (2004) 012004.

[12] G. Altarelli and G. Parisi: Nucl. Phys. B**126** (1997) 298.

[13] SMC, B. Adeva et al.: Phys. Rev. D**58** (1998) 112002.

[14] M. Hirai et al.: Phys. Rev. D**69** (2004) 054021.

[15] HERMES, H. Boettcher: *Proc. of the 10th International QCD Conference (QCD03)*, Montpellier (2003) (BB: hep-ph/0203155, LSS: hep-ph/0111257, GRV: hep-ph/0011215, AAC: hep-ph/0001046)

[16] J. D. Bjorken: Phys. Rev. **148** (1966) 1467, Phys. Rev. D**1** (1970) 1376.

[17] Particle data group: Phys. Lett. B**592** (2004) 1.

[18] J. Ellis and R. Jaffe: Phys. Rev. D**9** (1974) 1444, Dbf 10 (1974) 1669 (E).

[19] HERMES, A. Airapetian et al.: Phys. Rev. Lett. **90** (2003) 092002.

[20] E. D. Bloom and F. J. Gilman: Phys. Rev. D**4** (1971) 2901.

[21] M. Khandaker: *Proc. of the 12th International workshop on Deep Inelastic Scattering and QCD (DIS04)*, Strbske Pleso (2004).

[22] SMC, B. Adeva et al.: Phys. Lett. B**420** (1998) 180.

[23] HERMES, A. Airapetian et al.: Phys. Rev. D**71** (2005) 012003.

[24] A. Bravar et al.: Phys. Lett. B**421** (1998) 349.

[25] SMC, B. Adeva et al.: Phys. REv. D**70** (2004) 012002.

[26] HERMES, A. Airapetian et al.: Phys. Rev. Lett. **84** (200) 2584.

[27] COMPASS, C. Schill, Proc. of the 16th Int. Spin Symposium, Triest (2004).

[28] T. Gehrmann and W. J. Stirling, Z. Phys. C**65** (1994) 461.

[29] STAR, K. H. Ackermann et al.: Nucl. Instr. Meth. A**499** (2003) 624.

[30] STAR, S. Trentalange: *Proc. of the 12th International workshop on Deep Inelastic Scattering and QCD (DIS04)*, Strbske Pleso (2004).

[31] PHENIX, K. Adcox et al.: Nucl. Instr. Meth. A**499** (2003) 469.

[32] PHENIX, S. S. Adler et al.: Phys. Rev. Lett. **91** (2003) 241803.

[33] PHENIX, S. S. Adler et al.: Phys. Rev. Lett. **93** (2004) 202002.

[34] B. Jäger et al.: *Proc. of the 12th International workshop on Deep Inelastic Scattering and QCD (DIS04)*, Strbske Pleso (2004).

[35] M. Hirai and K. Sudoh: *Proc. of the 12th International workshop on Deep Inelastic Scattering and QCD (QCD04)*, Strbske Pleso (2004).

[36] M. Glück et al.: Phys. Rev. D**63** (2001) 094005.